Materials and Design 97 (2016) 204–212

Contents lists available at ScienceDirect

Materials and Design

journal homepage: www.elsevier.com/locate/matdes

Morphology-controlled synthesis of fluorapatite nano/microstructures via surfactant-assisted hydrothermal process

Juan Shen [a,b,*], Bo Jin [b], Qi-ying Jiang [a], Ya-min Hu [a], Xiao-yan Wang [c]

[a] School of Materials Science and Engineering, Southwest University of Science and Technology, Mianyang 621010, China
[b] State Key Laboratory Cultivation Base for Nonmetal Composites and Functional Materials, Southwest University of Science and Technology, Mianyang 621010, China
[c] Research Center for Nano-Biomaterials, Analytical &Testing Center, Sichuan University, Chengdu 610064, China

ARTICLE INFO

Article history:
Received 3 December 2015
Received in revised form 20 February 2016
Accepted 22 February 2016
Available online 23 February 2016

Keywords:
F-substituted hydroxyapatite
Surfactant
Hydrothermal

ABSTRACT

Uniform-large-sized F-substituted hydroxyapatite (FHAp) crystals with controllable morphologies were successfully synthesized via hydrothermal treatment by using double-facile surfactants. The products were characterized by X-ray diffraction, Fourier transform infrared spectroscopy, Raman spectroscopy, field-emission scanning electron microscopy, and high-resolution transmission electron microscopy. It was found that the size and morphology of FHAp crystals were drastically influenced by pH, precursor concentration and F^- content. The growth process was investigated by following time-dependent experiments. The possible growth process was also discussed.

1. Introduction

F-substituted hydroxyapatite (FHAp, $Ca_{10}(PO_4)_6F_x(OH)_{2-x}$, $x \le 2$) have been widely used in a promising potential candidate for increasing the bioactivity of dental restorative materials, bone regeneration, and drug delivery system [1–3]. It is well known that the performance of FHAp in the above applications depend on its physical and chemical properties, which are determined by morphology, size, dimensions, and chemical compositions [4]. Investigations to mimic the natural growth of hard tissue indicate that the synthesis of apatite-based biomaterials with various morphologies is the key step to completely understand their utility in industrial and biomedical applications [5–8]. Generally, crystallite formation can be influenced by temperature, solvents, pH, and organic growth modifiers, among others [9–11]. Among these influencing factors, organic growth modifiers are a crucial factor to determine the ultimate morphologies [12,13]. Various organic molecules, such as surfactants [14,15], ethylenediaminetetracetic acid (EDTA) [16,17], citrate [18,19], amino acids [20], and protein [21–23], have been used to synthesize hydroxyapatite (HAp) with various morphologies.

Usually, ethylenediaminetetracetic acid (EDTA) could control the nucleation and growth of FHAp due to modulate the concentration of uncomplexed calcium ions. Some studies about influence of EDTA addition on the morphologies of the FHAp products have been reported, which present elongated rod-like or whisker-like one-dimensional (1D) microcrystals in irregular shapes or their self-assembly three-dimensional (3D) microstructures, due to the fast growing direction along the *c*-axis [24–26]. Clarkson et al. synthesized FA nanorods/nanowires of different composition, shape, and size at low temperature or mild hydrothermal conditions using EDTA as a stabilizer in the precipitation solution [25]. Chen et al. fabricated FHAp products with flower-like, nanoprism, hexagonal nanorods, whisker and branch-like nanorod shape using Na_2EDTA as chelating reagent [26]. Similar observations have also been made in EDTA and citric acid surfactant-assisted hydrothermal synthesis of FHAp with different morphologies, such as hexagonal disks, hexagonal shuttles, hexagonal prisms, and icosahedrons [27]. Cationic surfactant cetyltrimethylammonium bromide (CTAB) also could control the growth of HAp as a result of the adsorption on HAp crystal surfaces through electrostatic attraction and structure complementarity, which possibly influence the morphological development of apatite crystals. When CTAB is chosen as a surfactant, it serves as a versatile soft template in HAp crystallization system, and hydroxyapatite particles including spheroid, long fibers, needle-like and rod-like morphologies are found [28,29]. Wang et al. modulated morphologies of hydroxyapatite from spheroid to long fibers through altering the reaction conditions and adding CTAB as a template [30]. Arami et al. mixed the CTAB with phosphate precursor and the CTAB–PO_4^{3-} complex formed rod-like micelles. The micelles acted as nucleating points for epitaxial growth of HAp nanostrips. However, little attention has been paid to morphology-controlled FHAp simultaneous using EDTA and CTAB. In addition, the mechanism of different morphologies based on organic growth modifier control remains poor known.

Therefore, we demonstrate a general strategy for the synthesis of FHAp nanostructures and microstructures by a hydrothermal route.

* Corresponding author at: School of Materials Science and Engineering, Southwest University of Science and Technology, Mianyang 621010, China.
E-mail address: sj-shenjuan@163.com (J. Shen).

http://dx.doi.org/10.1016/j.matdes.2016.02.091
0264-1275/

The cationic surfactant CTAB and EDTA are used as soft templates to modify the nucleation and growth process to obtain morphology-controlled FHAp crystals. The influence of the solution pH, precursor concentration and F^- content on particle nucleation and growth are studied. Moreover, the possible growth mechanism is also discussed based on the effects of surfactants on the system.

2. Experimental

All chemical regents were commercially available and used as received. FHAp samples were synthesized using the chelating-agent (EDTA) and surfactant (CTAB)-assisted hydrothermal method. Under magnetic stirring and at 60 °C, 1.1098 g of $CaCl_2$ and 3.7224 g of EDTA were dissolved in 100 mL of hot deionized water. The mixed solution was added to the surfactant-containing solution (2.1867 g of CTAB + 2.1578 g Na_2HPO_4 + 0.0420 g NaF) with 100 mL of deionized water. Drops of 3 M NaOH or HCl solution were then added to adjust the pH value. The mixture solution was concentrated to 100 mL and transferred to a 100 mL Teflon-lined stainless steel autoclave for hydrothermal treatment at 190 °C for 16 h. After being cooled down to room temperature, filtered, and washed with deionized water, the obtained powders were dried at a lyophilizer. The different reaction conditions and the products are summarized in Table 1.

The products were characterized and analyzed by X-ray diffraction (XRD), Fourier transform infrared (FTIR), field emission scanning electron microscopy (FESEM), energy-Dispersive X-ray (EDX) and high-resolution transmission electron microscopy (HRTEM). The XRD analysis was performed using a Rigaku D/max-RB X-ray diffractometer with CuKα radiation (λ = 1.5406 Å) at 35 kV and 60 mA. The 2θ range used was from 10° to 60° with a speed of 4°/min. FTIR spectra (KBr pellets) were recorded on a Nieolet 380 FTIR spectrometer. Raman spectra were taken on powder samples on a Renishaw inVia Raman spectrometer with 785 nm red laser irradiation. FESEM images were obtained on a Zeiss Ultra 55 scanning electron microscope at an accelerating voltage of 15 kV. Elemental analysis was conducted by using an Oxford X-Max 50 energy-dispersive X-ray spectrometer, which was directly connected to SEM. High-resolution transmission electron microscopy (HRTEM) and electron diffraction images were obtained on a Zeiss Libra 200FE transmission electron microscope at an accelerating voltage of 200 kV. Samples for transmission electron microscopy (TEM) were prepared by dispersing powdered FHAp products on carbon-coated Cu grids.

Table 1
Summary of experimental conditions versus the products.

Sample no.	$CaCl_2$ (mol/L)	EDTA (mol/L)	CTAB (mol/L)	Na_2HPO_4 (mol/L)	NaF (mol/L)	pH	Time (h)
1	0.1	0.1	0.06	0.15	0.01	3.6	16
2	0.1	0.1	0.06	0.15	0.01	4.0	16
3	0.1	0.1	0.06	0.15	0.01	5.2	16
4	0.1	0.1	0.06	0.15	0.01	6.1	16
5	0.1	0.1	0.06	0.15	0.01	9.7	16
6	0.3	0.3	0.18	0.45	0.03	6.1	5
7	0.3	0.3	0.18	0.45	0.03	6.1	16
8	0.1	0.1	0.06	0.15	0	9.7	16
9	0.1	0.1	0.06	0.15	0.002	9.7	16
10	0.1	0.1	0.06	0.15	0.02	9.7	16
11	0.1	0.1	0.06	0.15	0.002	6.1	16
12	0.1	0.1	0.06	0.15	0.01	6.1	16
13	0.1	0.1	0.06	0.15	0.02	6.1	16
14	0.1	0.1	0.06	0.15	0.01	6.1	0.17
15	0.1	0.1	0.06	0.15	0.01	6.1	0.5
16	0.1	0.1	0.06	0.15	0.01	6.1	1
17	0.1	0.1	0.06	0.15	0.01	6.1	10

3. Results and discussions

3.1. Influence of pH on FHAp crystals

Fig. 1 shows the XRD patterns of *as*-prepared FHAp samples under various pH values, indicating an overall crystalline nature of the products. All the diffraction peaks can be indexed to fluorapatite (FAp, JCPDS card No. 15-0876). The characteristic diffraction peaks are observed at 10.88°, 25.86°, 29.09°, 31.93°, 33.12°, 34.14°, 40.04°, 46.86° and 49.58°, corresponding to the (100), (002), (210), (211), (300), (202), (310), (222) and (213) planes of FHAp, respectively. The diffraction peaks of the as-prepared FHAp samples are similar to each other and clearly exhibit inconsistencies in the intensity reported in the JCPDS database (Fig. 1). The XRD patterns also show that there is a moderate difference from each other in the relative intensity based on (002), (211) and (300) peaks for five samples (Fig. 2), indicating the possibility of different preferential orientation growth of FHAp crystals under different pH conditions [26,27].

FTIR spectra of FHAp prepared at different pH values are shown in Fig. 3. The band at about 3576 cm^{-1} corresponds to the stretching vibration of the hydroxyl groups [31]. The wide absorption bands at around 3466 and the band at 1637 cm^{-1} are attributed to the adsorbed water [32]. The bands at 1103 and 1037 cm^{-1} are due to ν_3(P—O) asymmetric stretching mode, 973 cm^{-1} to ν_1(P—O) symmetric stretching mode, 613 and 569 cm^{-1} to ν_4(O—P—O) bending mode, and 479 cm^{-1} to ν_2(O—P—O) bending mode [33]. The weak bands at 1400 and 868 cm^{-1} are attributed to vibration modes of $\nu_3(CO_3^{2-})$ and $\nu_2(CO_3^{2-})$, respectively. Carbonate ions are a common impurity in apatite [32].

To evaluate the presence and the state of functional groups associated with FHAp, Raman spectra of the powders were also collected and are shown in Fig. 4. All the modes associated with the phosphate are observed ($\nu_1(PO_4^{3-})$, $\nu_2(PO_4^{3-})$, $\nu_3(PO_4^{3-})$, and $\nu_4(PO_4^{3-})$ bands) [33,34]. The phosphate modes at 1072 cm^{-1} ($\nu_3(PO_4^{3-})$), 1046 cm^{-1} ($\nu_3(PO_4^{3-})$), 959 cm^{-1} ($\nu_1(PO_4^{3-})$), 608 cm^{-1} ($\nu_4(PO_4^{3-})$), 590 cm^{-1} ($\nu_4(PO_4^{3-})$), 577 cm^{-1} ($\nu_4(PO_4^{3-})$), 445 cm^{-1} ($\nu_2(PO_4^{3-})$) and 432 cm^{-1} ($\nu_2(PO_4^{3-})$) are observed. It is also found that the $\nu_1(PO_4^{3-})$ band at 959 cm^{-1} is very intense and characteristic. The strongest peak at 959 cm^{-1} is a representative indication of crystalline hydroxyapatite. Combined FTIR and Raman analyses imply that all the powders are predominantly in the FHAp phase.

The morphology of the as-prepared samples was examined by FESEMs. When the pH value is 3.6, the individual FHAp crystal has a diameter in the range of 100 nm to 300 nm, a length of approximately 550 nm, and exhibits hexagonal prism-like morphology, which is

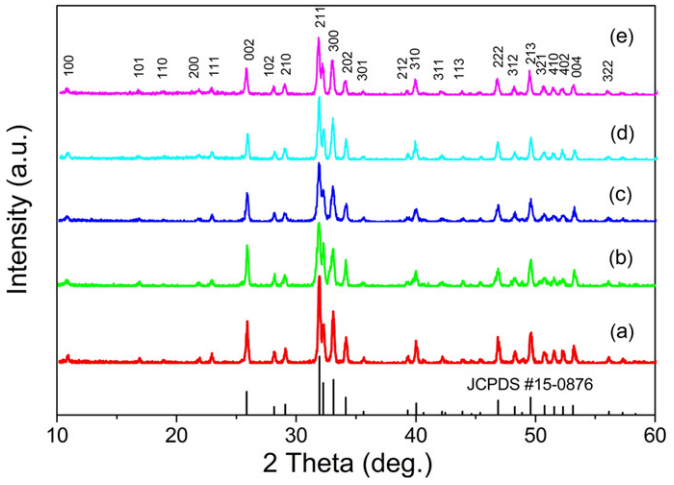

Fig. 1. XRD patterns of the samples obtained under various pH values: (a) pH = 3.6; (b) pH = 4.0; (c) pH = 5.2; (d) pH = 6.1; (e) pH = 9.7, and the standard data of FAp (JCPDS No. 15-0876) as a reference.